Research Square

Preprints are preliminary reports that have not undergone peer review.
They should not be considered conclusive, used to inform clinical practice,
or referenced by the media as validated information.

Investigation of the microstructure and mechanical properties of the Al-13.8 wt. % Mg 2 Si- Zr cylinder fabricated by the centrifugal casting

M. Ghayebloo

m.ghayebloo@ubonab.ac.ir

University of Bonab

Research Article

Keywords:

Posted Date: August 14th, 2026

DOI: https://doi.org/10.21203/rs.3.rs-8941357/v2

License: This work is licensed under a Creative Commons Attribution 4.0 International License.
Read Full License

Additional Declarations: No competing interests reported.

Investigation of the microstructure and mechanical properties of the Al-13.8 wt. % Mg_2Si-Zr cylinder fabricated by the centrifugal casting

M. Ghayebloo*

Department of Material Engineering, University of Bonab, Bonab, Iran

***m.ghayebloo@ubonab.ac.ir**

Abstract

Functionally graded materials are a new class of composites whose composition or microstructure changes continuously along a specific direction. One of the methods for producing the functional heterogeneity in the microstructure of cast materials is centrifugal casting. For this purpose, in this research, by centrifugal casting of Al-13.8wt.%Mg_2Si alloy and adding an appropriate amount of Al-5Zr, the changes in microstructure and mechanical properties in the radial direction of the cast cylinder were investigated. The microstructure of the cast cylinder without Zr showed columnar Al/Mg_2Si eutectic cells in the radial direction and the accumulation of primary Mg_2Si particles in the inner layer of the cylinder. In the next step, the effect of the addition of Zr on the microstructure and mechanical properties of the same alloy in the radial direction of the cast cylinders was investigated. The results showed that the addition of Zr led to a change in the morphology of the secondary phases of Mg_2Si from dendritic to cubic morphology and a finer size, and changed the fracture mode from cleavage to dimple fracture. Also, due to the enhancement in the amount of the Mg_2Si phase caused by the addition of Al-5Zr, the hardness of the sample containing Zr increased in all three layers. Tensile strength was enhanced in the three layers of the cylinder due to the increase in equiaxed eutectic cells and finer Mg_2Si particles.

Keywords: Functionally materials, centrifugal casting, Al-13.8 wt.%Mg_2Si-Zr alloy

1. Introduction

Functionally graded materials have a graded microstructure, physical and mechanical properties[1]. These materials have many applications in brake rotor discs, cylinder liners, pulleys, rocket nozzles, medical implants, armors and optical devices where high wear resistance and

hardness are required in combination with high bulk toughness[2,3]. This combination of properties may not be readily obtained in homogeneous aluminum matrix composites [3].

One of the suitable methods to eliminate the columnar region and create a coaxial cast structure is the addition of nucleating agents during solidification[4]. Various compositions have been used for nucleation in molten aluminum and its alloys. One of the most effective methods of improving the properties of aluminum alloys is grain refining by using the Al-Ti-B master alloys[5].

One such composition is the use of Al-5Zr as a nucleating agent[6]. Zirconium is a key alloying element, used mainly in the 2xxx and the 7xxx series of the aluminum alloys, where it contributes to dispersion enhancement and reduces the rate of dynamic recrystallisation[7,8]. Al-5Zr is a strong candidate for grain refinement of Al-Mg-Si alloys due to the formation of particles with high thermal stability and exceptional lattice compatibility with aluminum[9]. The Al_3Zr phase is more thermodynamically stable at high temperatures. It remains stable even near the melting point of aluminum, and its toxic effect is also less and reduces the nucleation performance to a lesser extent [7,10,11].

Various additives are available to control microstructural and grain refinement properties[12,13]. However, the role of the operating parameters of the casting process should not be overlooked[14–16]. One of the important variables in centrifugal casting to control the microstructure of the casting is the vibration of the melt during casting. The energy generated in the vibrations creates new nucleation sites due to the breakage of secondary arms in the melt, leading to a more even distribution of nucleation sites and faster solidification of the entire part[16]. Recently, functional materials reinforced with primary particles of Si, Al_2Cu, Al-$NiAl_3$, Al-Mg_2Si, Al-$TiAl_3$, Al-$NiAl_3$, Al-Al_3Zr, Al-5B, Al-7.2B, Al-4B-2Mg, Al-7Si-0.3Mg-TiB_2 have been produced based on the in-situ centrifugal casting method[2,17–23]. In this case, the effect of vibration and refiners on the microstructure of the hypoeutectic semi-solid slurry of the Al-Si alloy has been investigated[24].

This research aims to investigate the creation of a graded casting microstructure and mechanical properties of Al-13.8wt.%Mg_2Si and Al-13.8wt.%Mg_2Si-Zr cylinders fabricated by the centrifugal casting method. To our knowledge, the effect of Zr on the Al-Mg-Si eutectic alloy has not been investigated by the centrifugal method in details.

2. Experimental

The aim of this research is to investigate the feasibility of creating a graded cast microstructure in the eutectic Al-13.8wt.%Mg_2Si alloy by inducing functional nucleation using centrifugal casting. For this purpose, in the first stage, alloying with the desired composition was carried out. In the next stage, by remelting the prepared alloy and adding nucleating agents, cylindrical samples with functional microstructure were cast using a vertical centrifugal casting machine. Then, the microstructure of the cast cylindrical samples at different radial sections was quantitatively and qualitatively investigated. Figure 1 shows the stages of the experiments in this research.

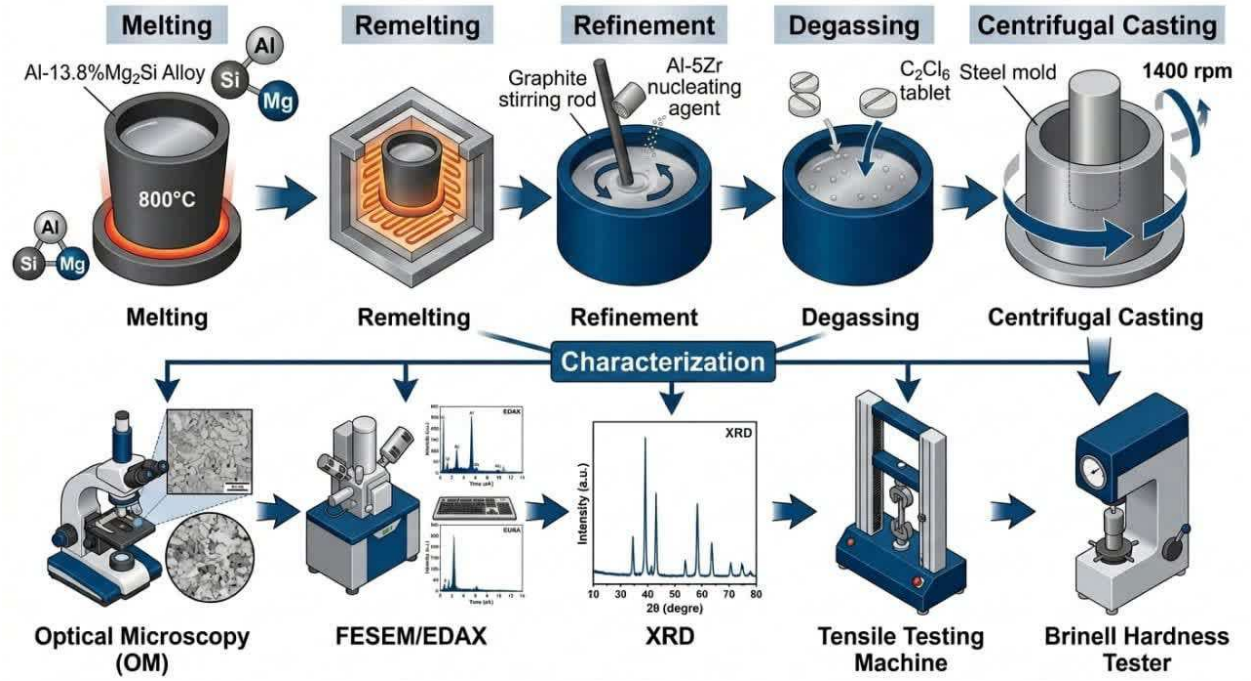


Figure 1. Schematic of the general process of conducting tests

2.1 Alloying of primary ingots

To prepare the initial Al-13.8wt.%Mg_2Si alloy (hereinafter referred to as Al-13.8%Mg_2Si for brevity), aluminum, magnesium, and silicon were used with a purity of 99.8%, 99.7%, and 99.9%, respectively.

For this purpose, aluminum was first melted in a graphite crucible using a ground furnace at 800 ^oC. Then, weighed silicon was added to the aluminum melt. Before adding weighed magnesium to the melt, the melt temperature was reduced to 740 ^oC due to the high vapor pressure of magnesium. Also, to compensate for losses due to magnesium burning, after performing multiple quantometers, the weight of magnesium was considered to be 15% more than the calculated weight ratio for the

alloy. After adding magnesium, the melt temperature was increased to 800 ºC and maintained at 800 ºC temperature for 15 minutes and cast into a metal mold. The final chemical composition of the alloy, as determined by quantometric analysis, is given in Table 1.

Table 1. Chemical composition of the alloy used (in weight percent)

Mg	Fe	Si	Al
7.76	0.16	5.13	rest

Since the mechanical properties of the samples were also measured in this work, the samples were cast with the least possible defects and porosity. Accordingly, the pre-alloyed ingots were remelted. Then, an Al-5Zr nucleating agent was used with an optimal percentage of 0.1% by weight and a density of $\rho = 2.776$ (g/cm^3). Initially, the nucleating agent was added to the eutectic alloy in an optimal percentage, and then centrifugal casting was performed.

After adding the nucleating agent, the melt was stirred well with a graphite rod for 5 minutes. Degassing was performed using hexachloroethane (C_2Cl_6) degassing tablets in different amounts and at different holding times. The results showed that the optimal condition for melt degassing was achieved using 0.5 wt.% of the dry degassing tablet with a holding time of 2 minutes.

2.2 Centrifugal Casting

To produce a graded alloy with a controlled gradient of microstructure and properties, a vertical centrifugal casting machine was used as shown in Figure 2 (a). After slag removal, the final casting operation was carried out in a vertical centrifugal casting machine equipped with a mold preheating system. The centrifugal casting machine had special capabilities including the ability to control the mold cooling rate during rotation, to create a variable mold rotation speed in the range of 0-3400 rpm, and to achieve isothermal solidification up to 700 ºC. The melt was poured into a rotating steel mold preheated to 300 ºC and a rotation speed of 1400 rpm. Before casting, a thin ceramic coating of 1 mm thickness was applied to the inner wall of the mold to reduce the solidification rate. After casting and solidification, functional cylinders with a length of 110 mm, an outer diameter of 90 mm, and a thickness of 15 mm were obtained as shown in Figure 2 (b).

The above-mentioned casting operation was also repeated for the casting of the Al-13.8%Mg_2Si alloy without adding a nucleating agent.



(a) (b)

Figure 2. (a)The inlet valve for the melt into the centrifugal casting machine, Al-13.8wt.%Mg 2 Si-Zr cylinder fabricated by the centrifugal casting method, (b) product cylinder

2.3 Sample preparation for metallography

Finally, the radial sections of the cylindrical samples, each 15 mm thick, were cut along the longitudinal direction and parallel to the rotation axis. After sanding and polishing, samples were etched with a 1% HF solution.

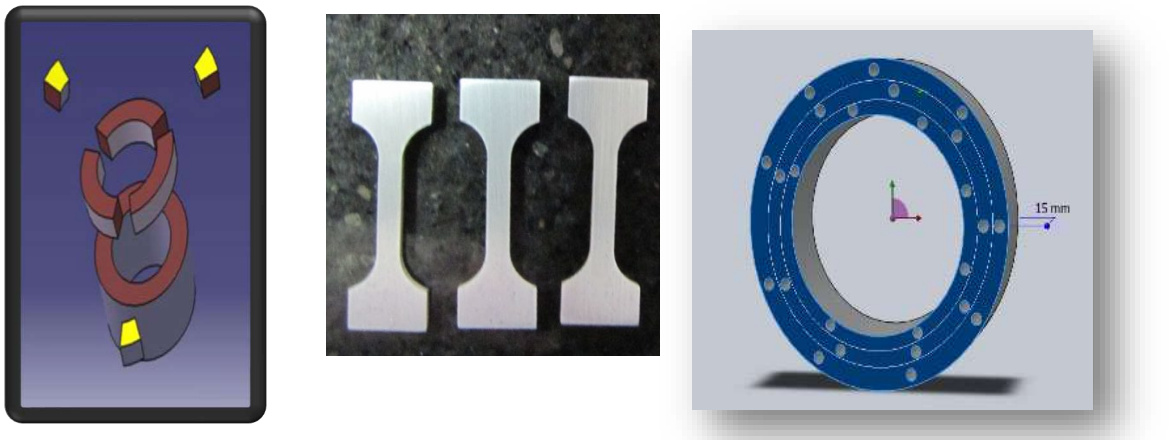
2.4 Microstructural and chemical composition characterizations

The microstructure of the radial sections (Figure 3 (a)) was studied using optical microscopy (OM) and FESEM equipped with EDAX (MIRA3 TESCAN).

2.5 Mechanical characterization

Tensile samples were cut from both the grain-refined and non-refined cast cylinders using a wire EDM machine under the JIS Z2201 No. 7 standard (Figure 3 (b)). Phase analysis was performed by an X-Ray Diffraction (XRD) spectrometer with step size: 0.02 and time per step: 0.5 s (with Cu Ka radiation, k = 0.15406 nm; 40 kV; Philips PW3710). Tensile tests were conducted using a Zwick/Roell testing machine with a 10-ton capacity. The tests were performed at room temperature with a jaw speed of 0.5 mm/min on the samples. The Brinell hardness test was performed with a

load of 125 kg for 10 s using the Kopa model hardness machine on different layers of cylinders (Figure 3 (c)).



(a) (b) (c)

Figure 3. (a) Schematic of metallographic sample preparation, (b) Flat tensile specimen used in tensile testing (according to JIS:Z2201 No7 standard), (c) Schematic of radial cross-sections of samples for Brinell hardness testing

3. Results and discussion

In order to identify the phases formed, the cast cylinders of Al-13.8%Mg_2Si and Al-13.8%Mg_2Si-Zr alloys were subjected to X-ray diffraction (XRD). However, since the content of Zr-containing phases was less than 5 wt%, they were not detected in the diffraction patterns. Figure 4 shows the XRD patterns of the Al-13.8%Mg_2Si and Al-13.8%Mg_2Si-Zr alloys after centrifugal casting. The identified phases include aluminum and Mg_2Si. The Mg_2Si phase is attributed to both primary (non-eutectic) particle and eutectic phases. In the Al-13.8%Mg_2Si-Zr alloy, the intensity of the Mg_2Si peaks is observed to increase, which is attributed to the addition of Zr to the eutectic alloy.

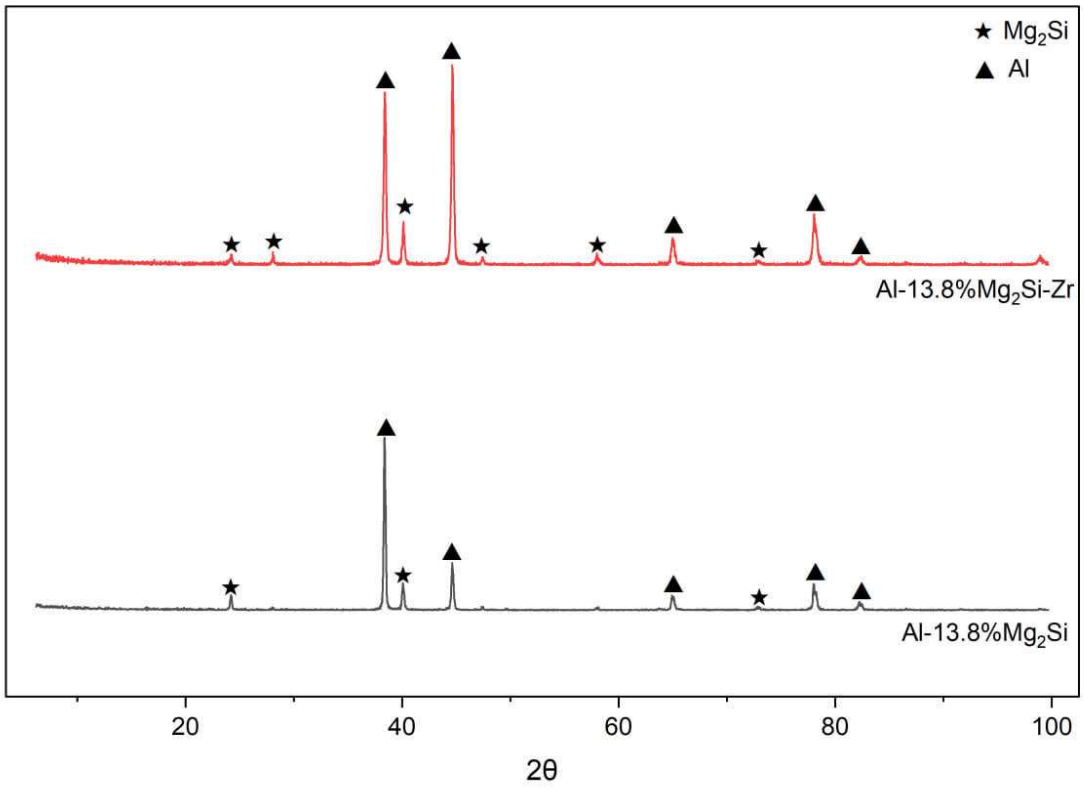


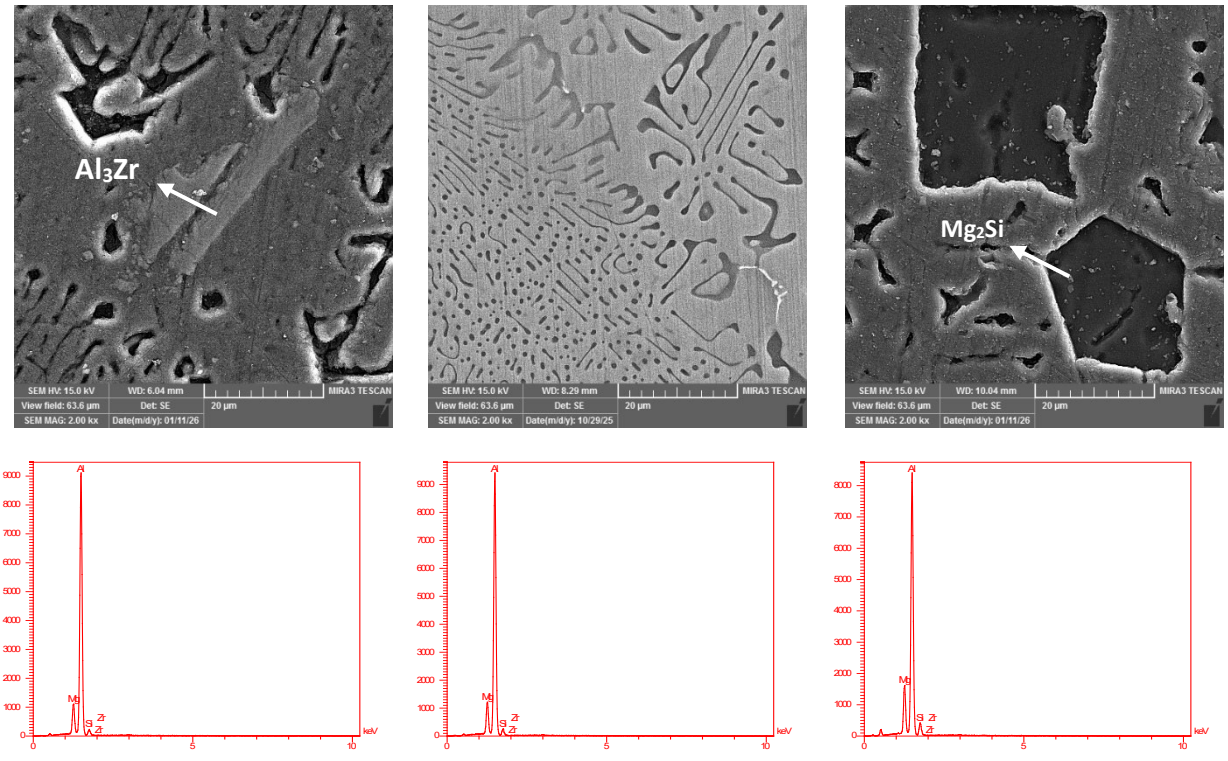
Figure 4. X-ray diffraction pattern of the Al-13.8%Mg_2Si and Al-13.8%Mg_2Si-Zr alloys after centrifugal casting

The equilibrium phase diagram of aluminum-zirconium has a peritectic reaction at 660.5 ºC. The solubility of zirconium in aluminum in the solid state at equilibrium temperature is about 0.28%. This solid solubility can reach 2 to 2.5% under non-equilibrium conditions. In practice, when the zirconium content increases from 0.16%, Al_3Zr intermetallic particles precipitate directly from the melt[25]. The Al_3Zr particles have excellent thermal stability due to their high negative formation energy (- 40 kj/mol) and high melting temperature (1580 ºC). Above 660.5 ºC temperature, there are L(Al) + Al_3Zr phases after undergoing a peritectic reaction[7].

$$L(Al) + Al_3Zr \Longrightarrow \alpha(Al) \qquad (1)$$

Since the melting temperature (800 ºC) is above the liquidus line, the formation of Al_3Zr phases is possible, allowing these phases to effectively play their nucleation role in the microstructure.

The Al-13.8%Mg_2Si alloy was cast via centrifugal casting in a preheated metal mold, with the addition of 0.1 wt. % Al-5Zr nucleating agent. The Al_3Zr intermetallic compound, with a density of 4.1 g/cm^3, was formed and fulfilled its nucleating role. Intermetallic phases such as Al_3Zr exhibit many attractive characteristics, including good oxidation resistance and high melting points. Due to its higher density (4.14 g/cm^3) compared to that of the molten alloy (2.57 g/cm^3), the Al_3Zr phase segregates against the centrifugal force toward the outer wall of the cylinder [26]. Figure 5 shows the EDAX spectra of the (a) outer, (b) middle and (c) inner layers of the Al-13.8%Mg_2Si-Zr alloy. The results indicate that Zr is present in all three layers, however, its content is higher in the outer layer.



Elt	W%
Mg	9.08
Al	86.97
Si	3.76
Zr	0.19

(a)

Elt	W%
Mg	9.30
Al	86.58
Si	4.03
Zr	0.09

(b)

Elt	W%
Mg	12.53
Al	80.31
Si	7.08
Zr	0.08

(c)

Figure 5. FESEM microstructural images and EDAX spectra of the (a) outer, (b) middle and (c) inner layers of the Al-13.8%Mg_2Si-Zr alloy

Figure6 shows optical microscope microstructure images of different radial sections. Images (a) to (c) represent the microstructure from the outer layer to the inner layer of the Al-13.8%Mg_2Si alloy cylinder, while images (d) to (f) represent the microstructure from the outer layer to the inner layer of the Al-13.8%Mg_2Si-Zr alloy cylinder. In the zirconium-free sample, (Figure6 (a), (b)), the eutectic cells grew in a columnar manner in the outer and middle layers. According to the optical micrographs of the eutectic Al-13.8%Mg_2Si alloy, the inner layer (Figure6 (c)) exhibits coarse eutectic layers along with primary Mg_2Si phase. In fact, the formation of coarse eutectic layers in the inner regions is attributed to the low solidification rate in these layers. Additionally, in Figure6 (c), black particles with a polyhedral morphology are observed, which correspond to primary Mg_2Si particles. Due to its lower density (1.95 g/cm³) compared to that of the molten alloy (2.6 g/cm³)[26], the Mg_2Si phase segregates against the centrifugal force toward the inner wall of the cylinder. The presence of the Mg_2Si phase in the inner layer indicates that the outer layers solidified earlier under non-equilibrium conditions. Subsequently, the Mg_2Si particles formed in the outer layers segregate toward the inner layers. It appears that the black phases present between the eutectic cells result from the formation of the ternary Al-Mg_2Si-Si eutectic, because within the eutectic cells, the stoichiometric ratio of silicon to magnesium in the eutectic Mg_2Si phase is 1:2, and the excess silicon is rejected to the cell boundaries, thereby increasing the silicon content at the boundaries.

Figure6 (d), corresponding to the outer layers, the distribution of needle-like phases is random. The higher cooling rate in the outer layer has led to the precipitation of these needle-like phases there. Li et al. reported that as the cooling rate increases, the morphology of the Al_3Zr phase becomes fine and blocky, while the coarse plate-like phase disappears[25]. In Figure6 (e), corresponding to the middle layer, the presence of zirconium and its segregation in the intercellular spaces has led to the formation of a coaxial eutectic cell microstructure. Indeed, upon adding zirconium to the base eutectic alloy, nucleation occurred throughout the melt, and the eutectic cells grew coaxially. In the Figure6 (f), corresponding to the inner layer, zirconium (Figure 7) prevented the growth of plate-like Mg_2Si particles and refined their size.

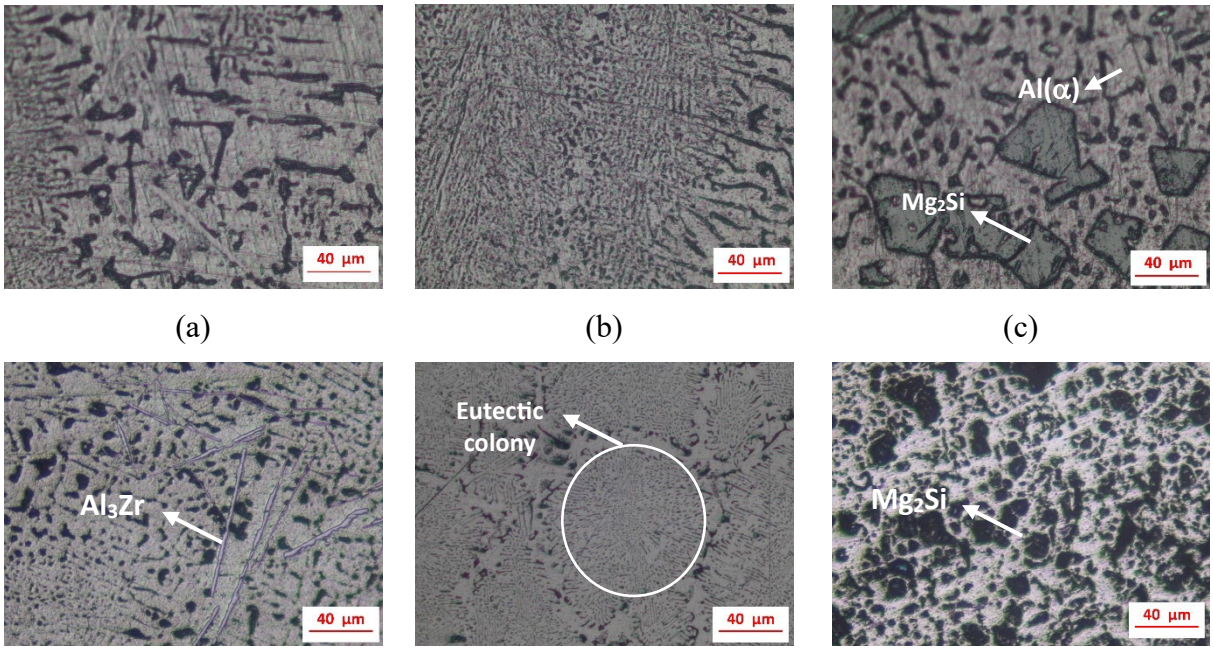
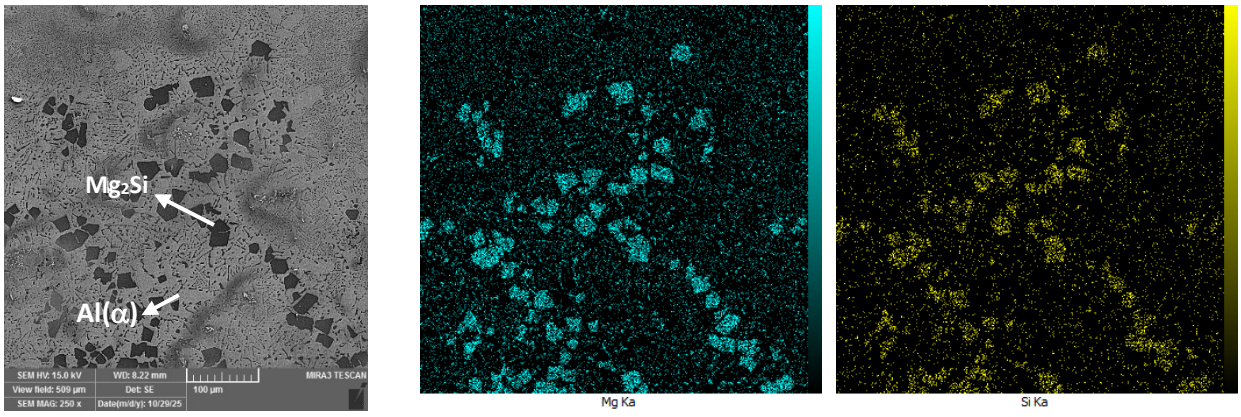


Figure 6. Optical microscope microstructures of different radial sections: images (a) to (c) show the microstructure from the outer layer to the inner layer of the Al-13.8%Mg_2Si alloy cylinder, and images (d) to (f) show the microstructure from the outer layer to the inner layer of the Al-13.8%Mg_2Si-Zr alloy cylinder

In Figure 7, mapping analysis images of the inner layers of Al-13.8 %Mg_2Si-Zr alloy are shown. The results indicate the Zr (show in red) is present in the structure of 13.8%Mg_2Si-Zr alloy cylinder.



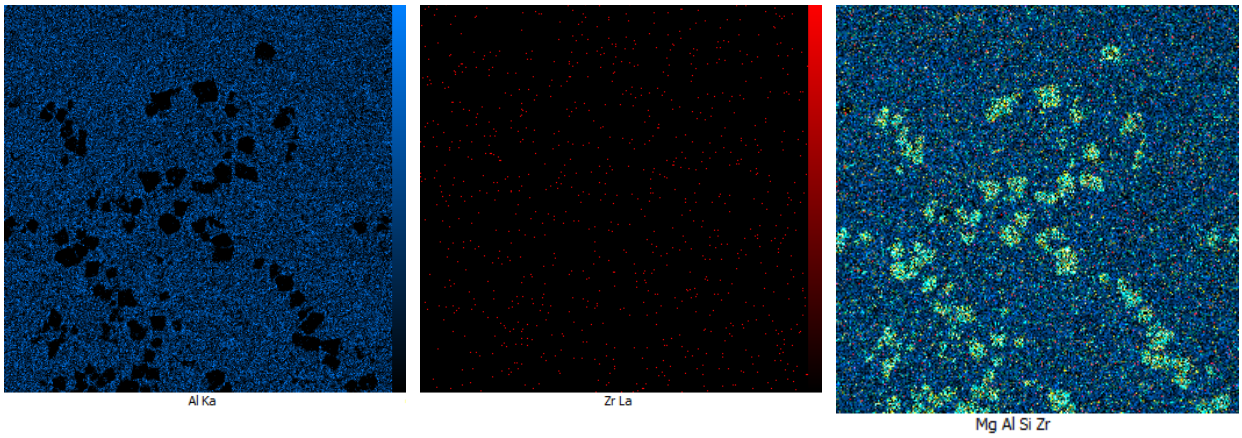
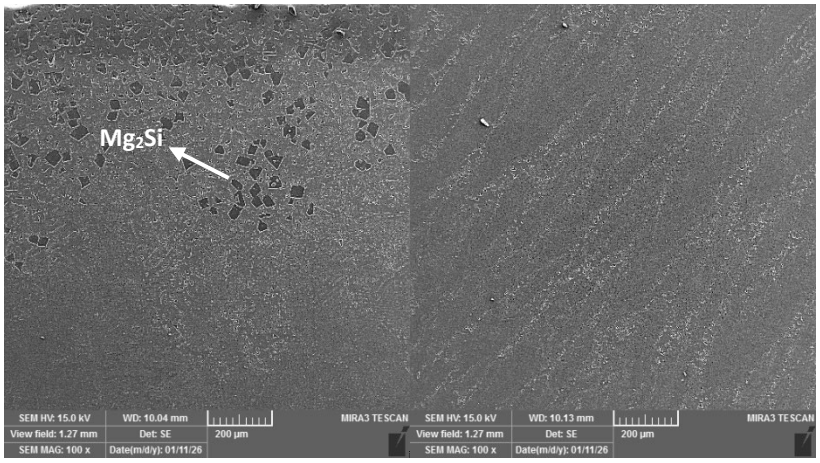


Figure 7. Mapping analysis images of the inner layers of the Al-13.8 %Mg_2Si-Zr alloy

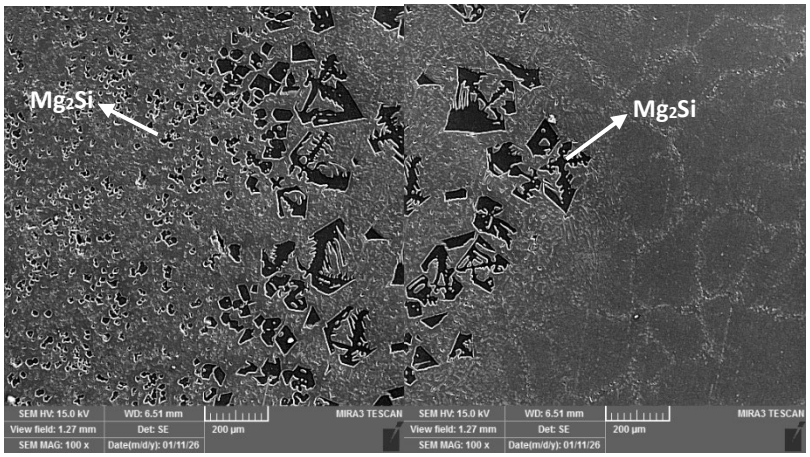
Figure 8, FESEM microstructure images of the middle and inner layers of centrifugally cast (a) Al–13.8% Mg_2Si cylinder and (b) Al–13.8% Mg_2Si-Zr cylinder are shown. The addition of Zr has a significant effect on the growth process of Mg_2Si particles, preventing the growth of certain planes in specific directions. As a result, the morphology of these particles changed to finer cubic shapes (Figure 8(b)). It has been reported Al_3Zr particles, with a strong pinning effect on grain boundaries, severely inhibit grain growth at high temperatures[27]. Azarbarmas et al. reported that there is no clear mechanism for the changes in the morphology of the Mg_2Si particles. This effect is probably due to an increase in the melting entropy of the Mg_2Si particles or to a change in their surface energy caused by lattice distortion resulting from the presence of additives in the Mg_2Si lattice[28]. However, in the transition region between the middle to inner layers, some of irregular polyhedral Mg_2Si particles with sizes of 180.73±17.61 μm can be observed. It seems that the formation of these irregular polyhedral Mg_2Si particles can be attributed to the low solidification rate in the inner layer of the cylinders. Table 2 shows the relationship between the Mg_2Si particle size in the Al-13.8%Mg_2Si and Al-13.8%Mg_2Si-Zr cast cylinders after centrifugal casting. It indicates that the addition of Zr can reduce the Mg_2Si particle size in the inner layer of the cast cylinders (as determined by Image J analysis) from 43.59±9.83 to 16.23±6.19 (μm).

Table 2. Relationship between Mg_2Si particle size in the inner layer of the Al-13.8%Mg_2Si and Al-13.8%Mg_2Si-Zr cast cylinders after centrifugal casting

	Inner layer (μm)
Al-13.8%Mg_2Si	43.59±9.83
Al-13.8%Mg_2Si-Zr	16.23±6.19



(a)



(b)

Figure 8. FESEM microstructural images of the middle and inner layers of centrifugally cast (a) Al–13.8% Mg_2Si cylinder and (b) Al–13.8% Mg_2Si-Zr cylinders

In this section, the Brinell hardness test results of the samples are examined. To this end, Figure 9 shows the Brinell hardness values of the functionally graded eutectic Al-13.8%Mg_2Si alloy without a nucleating agent and containing 0.1 wt. % Al-5Zr the nucleating agent, measured in different layers of the cylinder. It is observed that the hardness of the sample without a nucleating agent decreases from the outer layer to the inner layer. This can be attributed to the fact that, moving from the outer to the inner layer, the solidification rate decreases, leading to an increase in the interlamellar spacing of the eutectic layers and, consequently, a reduction in hardness. By examining the optical microscope microstructural images of the sample containing the Zr nucleating agent, it is observed that Zr refines the microstructure into equiaxed eutectic cells and

produces fine Mg_2Si particles. As a result, the Brinell hardness value has increased compared to the previous samples. Furthermore, in Figure 10, within the inner layer of the Al–13.8% Mg_2Si-Zr cylinder, crack deflection by the reinforcing Mg_2Si phases can be observed. Since the Mg_2Si phase size is smaller in this sample, it leads to greater crack deflection and, consequently, an increase in the Brinell hardness value.

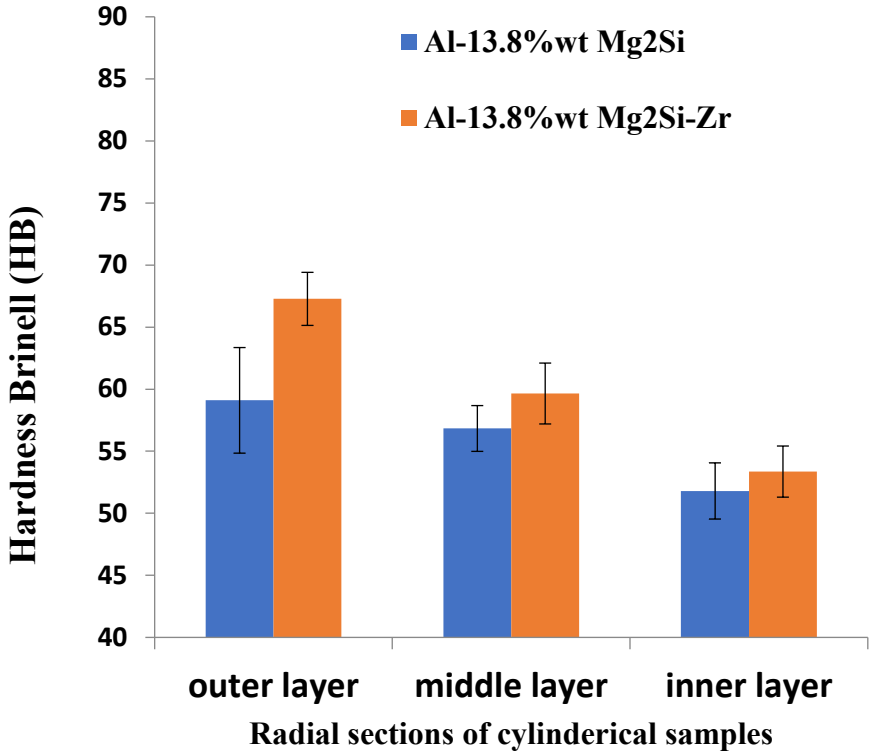


Figure 9 .Hardness variations in the outer, middle, and inner layers of the Al-13.8%Mg_2Si and the Al-13.8%Mg_2Si-Zr alloy cylinders

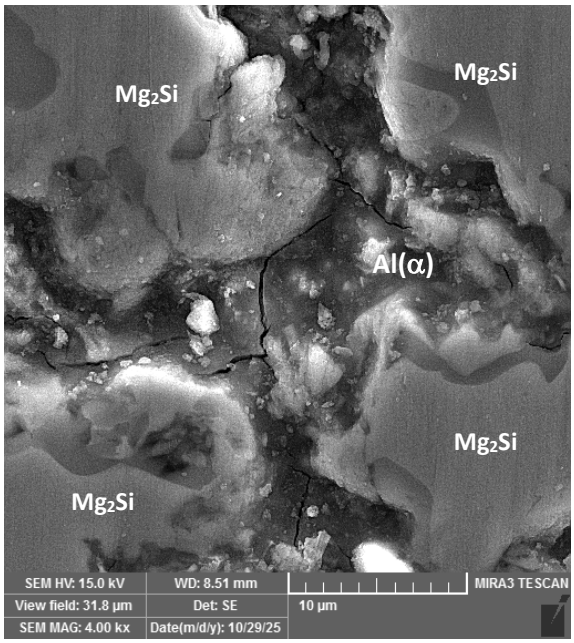


Figure 10. FESEM microstructural image of the Al-13.8%Mg_2Si-Zr sample in the inner layer

Figure 11 shows the tensile strength variations in the outer, middle, and layers of the Al-13.8%Mg_2Si and Al-13.8%Mg_2Si-Zr alloy cylinders. According to the results, it can be observed that the strength of the cast cylinders in all three layers (outer, middle and inner) has increased due to the addition of zirconium to the eutectic alloy, compared to the sample without zirconium. As mentioned earlier, the presence of fine needle-like Al_3Zr phases in the outer layer, the presence of equiaxed eutectic cells in the middle layer, and the presence of finer Mg_2Si particles in the inner layer have collectively contributed to the increase in the tensile strength of the samples.

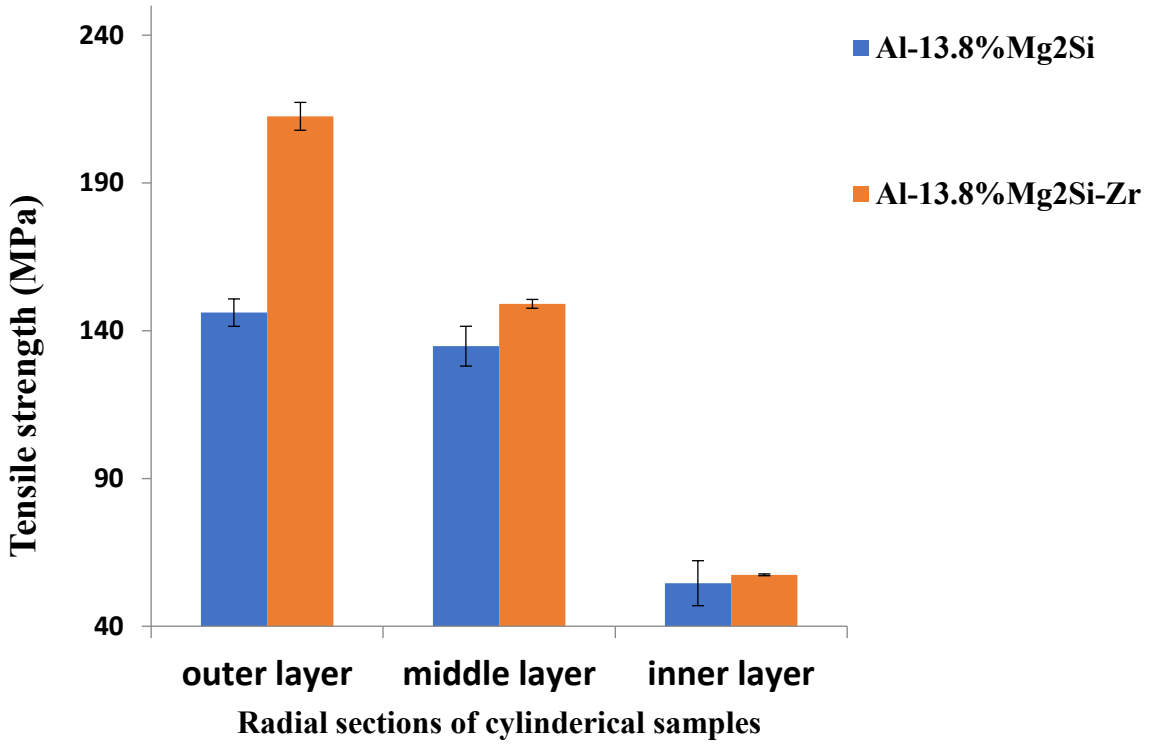


Figure 11. Tensile strength variations in outer, middle, and inner layers of the functionally graded Al-13.8%Mg_2Si and Al-13.8%Mg_2Si-Zr alloy cylinders

Figure 12 presents fracture surface images of different radial sections, from the outer layer to the inner layer, of both the Al-13.8%Mg_2Si and Al-13.8%Mg_2Si-Zr alloy cylinders. In the zirconium-free sample, coarse Mg_2Si particles cause embrittlement and lead to a fracture mode characterized primarily by cleavage. The sharp-edged secondary Mg_2Si particles act as stress concentrators, which reduce the fracture stress, and cracks propagate from these particles[29]. In the zirconium-containing sample, the reduction in the size of secondary Mg_2Si particles across the inner, middle, and outer layers of the cylinder results in the formation of dimples and incoherent Mg_2Si particles. These dimples form through void coalescence during plastic deformation, indicating ductile fracture in the composite. Second-phase particles are visible at the base of the dimples. Studies by other researchers have similarly shown an increase in dimple formation upon the addition of copper or beryllium to Al-Mg_2Si composites[28–30]. Furthermore, as shown in the Figure 10, the crack propagates from the interface between the matrix and the brittle Mg_2Si particles, leading to ductile fracture in the zirconium-containing sample.

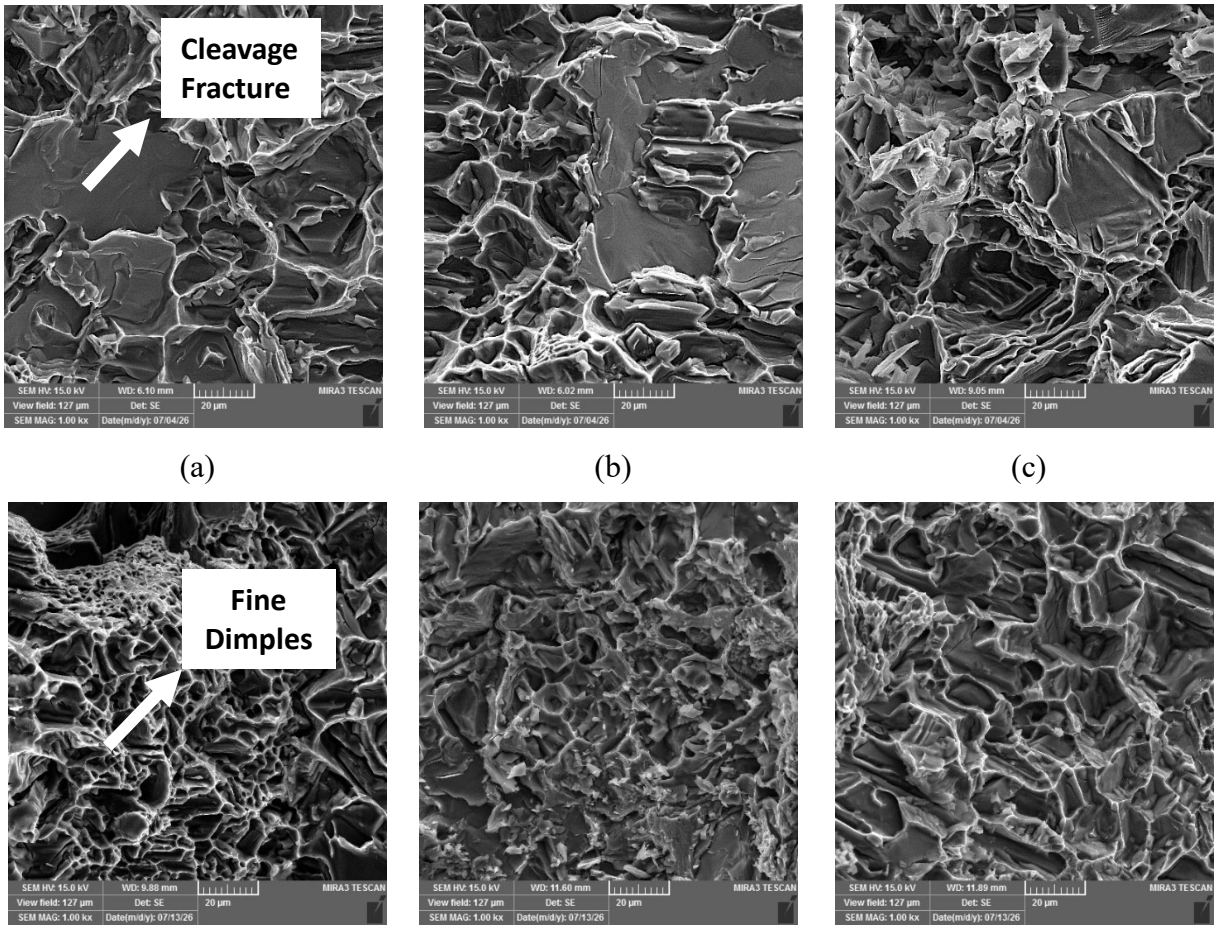


Figure 12. FESEM fracture surface images of different radial sections: (a) to (c) show the microstructure from the outer layer to the inner layer of the Al-13.8%Mg_2Si alloy cylinder, and (d) to (f) show the microstructure from the outer layer to the inner layer of the Al-13.8%Mg_2Si-Zr alloy cylinder

4. Conclusions

- The addition of Zr had a significant effect on reducing the size of eutectic cells and changing their morphology from columnar to equiaxed. It also led to a change in the morphology of the secondary Mg_2Si phases and reduced their size from 43.59±9.83 μm to 16.23±6.19 μm.
- The Addition of Zr changed the fracture from cleavage fracture (in the sample without Zr) to dimple fracture (in the sample with Zr).

- The Brinell hardness value of the eutectic alloy decreased from 59.1 HB (outer layer) to 53.36 HB (inner layer), while the Brinell hardness of the Zr-containing eutectic alloy decreased from 67.27 HB (outer layer) to 53.36 HB (inner layer).
- The Tensile strength of the eutectic alloy, due to the presence of columnar eutectic cells and larger Mg_2Si particles, varies from 146.12 MPa (outer layer) to 54.56 MPa (inner layer). In contrast, the tensile strength of the Zr-containing eutectic alloy, owing to equiaxed eutectic cells and finer Mg_2Si particles, varies from 212.55 MPa (outer layer) to 57.39 MPa (inner layer). The most pronounced effect of Zr addition is observed in the outer layer of the Al-13.8%Mg_2Si alloy.

Acknowledgement

We are thankful to Sahand university of technology for their casting supports. We are also grateful to university of Bonab for its financial support (Grant No.7479)

References

[1] Suresh S and Mortensen A 1997 Functionally graded metals and metal-ceramic composites: Part 2 Thermomechanical behaviour *Int. Mater. Rev.* **42** 85–116

[2] Kumar S, Subramaniya Sarma V and Murty B 2010 Functionally graded Al alloy matrix in-situ composites *Metall. Mater. Trans. A* **41** 242–54

[3] Melgarejo Z H, Suárez O M and Sridharan K 2006 Wear resistance of a functionally-graded aluminum matrix composite *Scr. Mater.* **55** 95–8

[4] Mohanty P and Gruzleski J 1995 Mechanism of grain refinement in aluminium *Acta Metall. Mater.* **43** 2001–12

[5] Chen T, Wang R, Ma Y and Hao Y 2012 Grain refinement of AZ91D magnesium alloy by Al–Ti–B master alloy and its effect on mechanical properties *Mater. Des.* **34** 637–48

[6] Wu J, Ruan Q, Chen S, Meng C, Xu Z, Wei C, Tang H and Wang J 2022 Insights into poisoning mechanism of Zr by first principle calculation on adhesion work and adsorption energy between TiB2, Al3Ti, and Al3Zr *Metals* **12** 286

[7] Kapinos D, Augustyn B, Boczkal S, Limanówka K, Płonka B, Garbacz-Klempka A, Piękoś M and Kozana J 2025 Influence of Zr on Al-Ti-B-Based Grain Refiners in AlSiMgCuZr Alloy *Materials* **18** 3000

[8] Zhang L, Yang L, Zhao J, Shen Z, Li Q, Jiang H and He J 2024 A novel insight toward Zr poisoning on grain refinement of Al–5Ti–1B and its solution *Metall. Mater. Trans. B* **55** 2765–75

[9] Elasheri A, Elgallad E M, Parson N and Chen X-G 2023 Nucleation and transformation of Zr-bearing dispersoids in Al–Mg–Si 6xxx alloys *J. Mater. Res.* **38** 696–707

[10] Pang X, Yang L, Yang J, Pang M, Xu Z, Li A, Wei B and Tang H 2023 Understanding the poisoning mechanisms of Si and Zr atoms on L12 Al3Ti (111) surface: A first-principles investigation *Vacuum* **210** 111891

[11] Li D, Yan X, Fan Y, Liu G, Nie J, Liu X and Liu S 2023 An anti Si/Zr-poisoning strategy of Al grain refinement by the evolving effect of doped complex *Acta Mater.* **249** 118812

[12] Zhiguo L, Shengping W, Hui H, Wu W and Zuoren N 2023 Grain refinement of aluminum and aluminum alloys by Sc and Zr

[13] Bolibruchová D, Matejka M, Širanec L and Švec M 2024 Zr as an alternative grain refiner in the novel AlSi5Cu2Mg alloy *Metals* **14** 581

[14] Chirita G, Soares D and Silva F 2008 Advantages of the centrifugal casting technique for the production of structural components with Al–Si alloys *Mater. Des.* **29** 20–7

[15] Chirita G, Stefanescu I, Cruz D, Soares D and Silva F 2010 Sensitivity of different Al–Si alloys to centrifugal casting effect *Mater. Des.* **31** 2867–77

[16] Chirita G, Stefanescu I, Soares D, Cruz D and Silva F 2008 Centrifugal casting features/metallurgical characterization of aluminum alloys AIP Conference Proceedings vol 973 (American Institute of Physics) pp 598–603

[17] Watanabe Y, Kawamoto A and Matsuda K 2002 Particle size distributions in functionally graded materials fabricated by the centrifugal solid-particle method *Compos. Sci. Technol.* **62** 881–8

[18] Raghunandan S, Hyder J A, Rajan T, Prabhu K N and Pai B 2012 Processing of primary silicon and Mg2Si reinforced hybrid functionally graded aluminum composites by centrifugal casting Materials Science Forum vol 710 (Trans Tech Publ) pp 395–400

[19] Ferreira S, Rocha L, Ariza E, Sequeira P, Watanabe Y and Fernandes J 2011 Corrosion behaviour of Al/Al3Ti and Al/Al3Zr functionally graded materials produced by centrifugal solid-particle method: Influence of the intermetallics volume fraction *Corros. Sci.* **53** 2058–65

[20] Tabushi K, Sato H and Watanabe Y 2010 Effect of casting condition on density and hardness gradients of Al-Al2Cu alloy FGM fabricated by centrifugal in situ method Materials Science Forum vol 631 (Trans Tech Publ) pp 449–54

[21] El Hadad S, Sato H, Sequeira P, Watanabe Y and Oya-Seimiya Y 2010 Effects of the processing temperature of centrifugal casting on the mechanical properties of Al-Al3Ti FGMs Materials Science Forum vol 631 (Trans Tech Publ) pp 373–8

[22] Duque N B, Melgarejo Z H and Suarez O M 2005 Functionally graded aluminum matrix composites produced by centrifugal casting *Mater. Charact.* **55** 167–71

[23] Nandam S H, Sankaran S and Murty B 2011 Precipitation kinetics in Al-Si-Mg/TiB2 in-situ composites *Trans. Indian Inst. Met.* **64** 123

[24] Ping A 2008 Effects of vibration and grain refiner on microstructure of semisolid slurry of hypoeutectic Al-Si alloy *Trans. Nonferrous Met. Soc. China* **18** 842–6

[25] Li Z, Zhang W, Fan S and Jiang Q 2023 Effect of Cooling Rate and Remelting Temperature on the Solidification Structure of Al-5Zr Master Alloy *Metals* **13** 749

[26] El Hadad S, Sato H, Sequeira P, Watanabe Y and Oya-Seimiya Y 2010 Effects of the processing temperature of centrifugal casting on the mechanical properties of Al-Al3Ti FGMs Materials Science Forum vol 631 (Trans Tech Publ) pp 373–8

[27] Sreekumar V and Eskin D 2016 A new Al-Zr-Ti master alloy for ultrasonic grain refinement of wrought and foundry aluminum alloys *Jom* **68** 3088–93

[28] Azarbarmas M, Emamy M, Rassizadehghani J and Alipour M 2011 The influence of beryllium addition on the microstructure and mechanical properties of Al–15% Mg2Si in-situ metal matrix composite *Mater. Sci. Eng. A* **528** 8205–11

[29] Zou X, Liu T, Liu W, Wang F, Li Y, Su R and Shi L 2025 The effect of Cu on microstructure, mechanical properties and fracture behavior of Al-15% Mg2Si composite *J. Alloys Compd.* **1012** 178497

[30] Azarbarmas M, Emamy M and Alipour M 2011 Study on fracture behaviour of Al–15% Mg2Si metal matrix composite with and without beryllium additions *J. Mater. Sci.* **46** 6856–62

Statements and Declarations

Competing Interests

The authors have no relevant financial or non-financial interests to disclose.

Author Contributions

All authors contributed to the study conception and design. Material preparation, data collection and analysis were performed by Masomeh Ghayebloo. The first draft of the manuscript was written by Masomeh Ghayebloo and all authors commented on previous versions of the manuscript. All authors read and approved the final manuscript.

Funding Declaration

The author(s) received financial support (number :7479) for the research.

Supplementary Files

This is a list of supplementary files associated with this preprint. Click to download.

- Tables.docx